Mosaic *BRAF* Fusions Are a Recurrent Cause of Congenital Melanocytic Nevi Targetable by MAPK Pathway Inhibition

Sara Barberan Martin[1,2,9], Satyamaanasa Polubothu[2,3,9], Alicia Lopez Bruzos[1,2,9], Gavin Kelly[4], Stuart Horswell[5], Aimie Sauvadet[1,2], Dale Bryant[1,2], Davide Zecchin[1,2], Melissa Riachi[1,2], Fanourios Michailidis[1,2], Amir Sadri[6], Noreen Muwanga-Nanyonjo[1,2], Pablo Lopez-Balboa[3], Nicole Knöpfel[1,2,3], Neil Bulstrode[3], Alan Pittman[7], Iwei Yeh[8] and Veronica A. Kinsler[1,2,3]

Among children with multiple congenital melanocytic nevi, 25% have no established genetic cause, of whom many develop a hyperproliferative and severely pruritic phenotype resistant to treatment. Gene fusions have been reported in individual cases of congenital melanocytic nevi. We studied 169 patients with congenital melanocytic nevi in this study, 38 of whom were double wild type for pathogenic *NRAS/BRAF* variants. Nineteen of these 38 patients had sufficient tissue to undergo RNA sequencing, which revealed mosaic *BRAF* fusions in 11 of 19 patients and mosaic *RAF1* fusions in 1 of 19. Recurrently, fusions involved the loss of the 5′ regulatory domain of *BRAF* or *RAF1* but preserved the kinase domain. We validated all cases and detected the fusions in two separate nevi in 5 of 12 patients, confirming clonality. The absence of the fusion in blood in 8 of 12 patients indicated mosaicism. Primary culture of *BRAF*-fusion nevus cells from 3 of 12 patients demonstrated highly increased MAPK activation, despite only mildly increased *BRAF* expression, suggesting additional mechanisms of kinase activation. Trametinib quenched MAPK hyperactivation in vitro, and treatment of two patients caused rapid improvement in bulk tissue, improving bodily movement and reducing inflammation and severe pruritus. These findings offer a genetic diagnosis to an additional group of patients and trametinib as a treatment option for the severe associated phenotypes.

INTRODUCTION

Congenital melanocytic nevi (CMN) are moles present from birth, termed CMN syndrome when associated with other features. Known recurrent causes of CMN are mosaic heterozygous missense pathogenic variants in *NRAS* (Kinsler et al., 2013) and *BRAF* (Etchevers et al., 2018) at 68 and 7% frequencies, respectively, in the largest prospective study (Polubothu et al., 2020), with the remaining 25% unknown. The condition is thus monogenic but mosaic, with the causative variant occurring in a single cell during embryonic or fetal development. The highly variable severity of the phenotype is likely related to the timing of the variant and the multipotency of the variant cell, among many other potential factors (reviewed in Kinsler et al. [2020]), with earlier mutagenesis generally thought to lead to more severe disease affecting more tissue types. Thus far, the causative clonal mosaic genotype has not been linked to disease severity, in so much that there have been no differences between *NRAS* and *BRAF* missense variants or the unknown group in the incidence of associated neurological abnormalities or incidence of melanoma in childhood, although numbers for melanoma are small (Polubothu et al., 2020). However, there have been early indications that the genotype may be related to the behavioral phenotype of the skin lesions, with *BRAF*[V600E] CMN more likely than NRAS CMN to present with multiple benign nodules (Polubothu et al., 2020; Salgado et al., 2015). In addition, the unknown genotype (wild-type) group appeared to us to contain some of the most proliferative and symptomatic cutaneous phenotypes. We have termed this phenotype hyperproliferative, as defined as recurrently developing distinct nodular or widespread proliferative areas within the CMN in the postnatal period. In addition, these areas are typically clinically inflamed (erythematous, warm), often hairless, and usually highly pruritic.

Gene fusions have previously been reported in a small number of cases of CMN and, in two cases, have been demonstrated in more than one nevus from the same patient. This demonstration of clonality within a patient helps to

[1]*Mosaicism and Precision Medicine laboratory, The Francis Crick Institute, London, United Kingdom;* [2]*Genetics and Genomic Medicine, UCL Great Osmond Street Institute of Child Health, London, United Kingdom;* [3]*Paediatric Dermatology, Great Ormond Street Hospital for Children, London, United Kingdom;* [4]*Bioinformatics and Biostatistics, The Francis Crick Institute, London, United Kingdom;* [5]*Open Targets, Welcome Sanger Institute, Cambridge, United Kingdom;* [6]*Plastic and Reconstructive Surgery, Great Ormond Street Hospital for Children and UCL Great Osmond Street Institute of Child Health, London, United Kingdom;* [7]*Genetics Research Centre (A.P.), St George's University of London, London, United Kingdom; and* [8]*Dermatology and Pathology, University of California, San Francisco, San Francisco, California, USA*

[9]*These authors contributed equally to this work.*

Correspondence: Veronica A. Kinsler, Mosaicism and Precision Medicine laboratory, The Francis Crick Institute, 1 Midland Road, London NW1 1AT, United Kingdom. E-mail: v.kinsler@ucl.ac.uk

Abbreviations: CMN, congenital melanocytic nevi; ERK, extracellular signal−regulated kinase; RNAseq, RNA sequencing

Received 1 February 2023; revised 16 May 2023; accepted 6 June 2023; accepted manuscript published online 15 September 2023; corrected proof published online 18 November 2023

define likely causality in the context of the multiple non-causative somatic mutations that can be detected in skin nevi. The first description was of two patients with translocations involving *BRAF* in a single sample each (Dessars et al., 2007), followed by single cases of likely causative *RAF1* and *ALK* fusions in two samples from each patient (Martins da Silva et al., 2019) and single cases with single samples of *RAF1*, *BRAF* (two cases), and *RASGRF2* fusions (Baltres et al., 2019; Houlier et al., 2021; Mir et al., 2019; Molho-Pessach et al., 2022). As to the precausal somatic mutational origins of CMN, recent data suggest a contribution from mismatch repair in some patients (Wei et al., 2023). Over the last 15 years, we have collected a cohort of patients with CMN for in-depth phenotypic and genotypic studies and undertook whole transcriptome RNA sequencing (RNAseq) on 19 of 169 who were wildtype for *NRAS* and *BRAF* missense pathogenic variants and for whom we still had sufficient tissue. We were particularly interested in learning more about this group of patients because the common occurrence of postnatal proliferation and intractable pruritus is classically resistant to treatments.

RESULTS

Mosaic *BRAF* fusions are a recurrent cause of multiple CMN
A total of 15 different mosaic gene fusions were identified in CMN tissue samples from 12 of 19 patients (7% of the total 169 patient cohort, clinical examples Figure 1a–c): 13 fusions involving *BRAF* in 11 patients and two involving *RAF1* in one patient (Figure 2a and b and Supplementary Table S1). The *BRAF* fusions identified consisted of both inter (11 of 13) and intrachromosomal rearrangements (2 of 13), whereas both *RAF1* fusions were intrachromosomal (two of two) (Figure 2c). All patients but one (10 of 11) presented at least one *BRAF* fusion consisting of the 5′ regulatory region of the partner gene fused to the 3′ portion of *BRAF*, which encodes for the tyrosine kinase domain (5′partner-3′ *BRAF*). Within those 10 patients, two (patients 3 and 10) had an additional *BRAF* fusion in the opposite direction (5′BRAF-3′ partner) involving the same (patient 10) or a different (patient 3) partner gene. In the one remaining patient (patient 11), the only identifiable fusion was 5′ *BRAF* fused to the 3′ partner gene (5′BRAF-3′partner) (Figure 2a). For the single *RAF1* patient (patient 12), we identified two fusions involving the same partner gene, one in each orientation (Figure 2b). Examples of sashimi plots showing the spanning and junction reads supporting the rearrangements are shown in Figure 2d and e and Supplementary Figure S1.

Mosaic *BRAF* fusions have varied but some recurrent breakpoints
The location of the breakpoints within *BRAF* varied between fusions, although a breakpoint at the start of exon 9 was recurrent and the most common (8 of 13 fusions) (Figure 2a and Supplementary Table S1). For *RAF1*, two different breakpoints were found in the two fusions (Figure 2b and Supplementary Table S1). Assessment of break points in the fusion genes did not implicate segmental duplications or SINE (short interspersed nuclear element)/LINE (long interspersed nuclear element) involvement in most cases as assessed by RepeatMasker (Kent et al., 2002) (Supplementary Figure S2).

Mosaic *BRAF* fusions have multiple partner genes that contain predicted dimerization domains
Ten different partner genes were identified (*AGAP3*, *AKAP9*, *EEA1*, *GOLGA4*, *LCA5*, *MIER3*, *PHIP*, *QKI*, *SEC31A*, *STRN3*). Of those, only *EEA1* and *GOLGA4* were recurrent partners (Figure 2a and b). The functional domains contributed by each partner include the promoter regions, which would be predicted to drive expression of the *BRAF/RAF1* kinases. A diverse mixture of other domains is predicted in silico in partner genes, in particular dimerization domains in 10 of 15 fusions (Figure 2a and b).

Mosaic *BRAF* fusions are associated with the hyperproliferative CMN phenotype
The phenotypic description of the 19 patients included in this study is detailed in Supplementary Table S1. The presence of a *BRAF/RAF1* fusion is significantly associated with a hyperproliferative phenotype ($P < 0.001$) (Supplementary Figure S2a−c) observed in 8 of 12 patients (66%) compared with that observed in 6 of 119 patients (5%) from the *NRAS* variant cohort. Other factors to note in *BRAF/RAF1* fusion patients are the chronic intractable pruritus interfering with everyday life (in 8 of 12) and the frequent requirement for surgical intervention for debulking of the tissue overgrowth and its associated pruritus in 6 of 12.

BRAF-fusion CMN exhibits histological features similar to *BRAF*-fusion acquired nevi
Tissue sections were available for review for 8 of 12 fusion patients. Multiple blocks were reviewed from the same patient when available (four of eight). In total, 25 different blocks were reviewed from eight patients (Supplementary Table S2). Key defining features identified in this cohort were desmoplasia and fibrosis in six patients (cords in whorled fibrosis in six of six cases and buckshot fibrosis and cords in whorled fibrosis in one of six) (Figure 1d and e). This has been previously reported in acquired *BRAF*-fusion melanocytic tumors (Perron et al., 2018). Some cases exhibited small melanocytes (n = 4 of 8), whereas some cases also exhibited a more spitzoid cytomorphology (n = 3 of 8) (Figure 1f). One patient showed evidence of pagetoid melanocytes.

Mosaic gene fusions are validated by alternative methods, and clonality is confirmed within patients
Fusions were validated by PCR and Sanger sequencing of patient CMN tissue cDNA using fusion-specific primers (Figure 3a and b and Supplementary Table S1). All RNAseq-detected fusions were confirmed (Supplementary Figure S3). In all patients where samples were available from more than one physically distinct nevi (5 of 12), the same fusion was in addition validated in each sample from the same patient (Figure 3a), demonstrating clonality and likely disease causality. Blood samples were available for eight patients, in which the absence of the fusion was demonstrated by an absence of amplification by PCR (Figure 3a), as is the pattern for mosaicism in CMN of other genotypes.

As a further validation method, we stained patient-derived nevus cells (from patients 1, 2, and 3) with a *BRAF* break-apart probe (Figure 3c). The absence of colocalization of the two probes surrounding the genomic region of *BRAF* demonstrates the presence of a
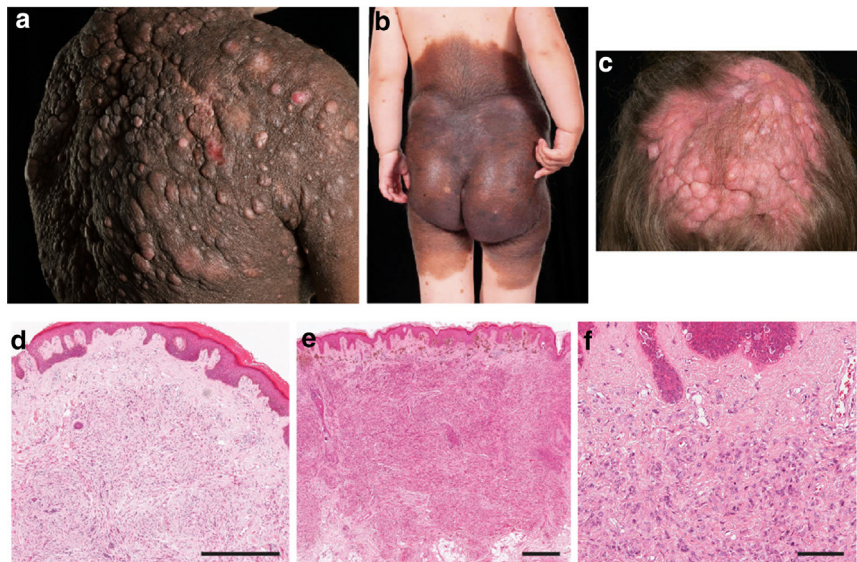
Figure 1. Clinical and histological features of patients with CMN harboring *BRAF* fusions. (**a**) Patient with hyperproliferative and multinodular phenotype, with excoriations demonstrating evidence of chronic pruritus. (**b**) Patient with more diffusely bulky and progressive hyperproliferation, also chronically pruritic. (**c**) Patient with hyperproliferative and multinodular phenotype on the scalp, also chronically pruritic. (**d**) Nevus with adjacent proliferative nodule area with slightly epithelioid melanocytes. (**e, f**) CMN demonstrating storiform fibrosis with a high degree of cellularity. Parents/guardians consented to the publication of patient images. Bar = 500 μm in **d** and **e** and 100 μm in **f**. CMN, congenital melanocytic nevi.

rearrangement involving *BRAF* in the three cell lines (arrowheads in Figure 3c). No rearrangement is present in the melanocyte control cell line (Hermes-1) as seen by colocalization of the probes.

BRAF fusions are associated with increased *BRAF* expression and hyperactivation of the MAPK pathway

Considering that most of the *BRAF* fusions identified involved loss of the autoinhibitory domain of *BRAF*, likely leaving the control of its expression to the partner gene (Figure 2a and b), we sought to investigate whether the baseline levels of expression of *BRAF* were altered by the fusion events. Assessing expression levels from the RNAseq was not thought to be accurate. The reasons for this are twofold. First, the gene fusions are mosaic; they are only present in nevus cells and not in other cell types in affected skin biopsy, whereas the bulk RNAseq data were from whole-skin biopsies. Differences in expression due to the fusion may therefore be lost within the bulk tissue. Second, only the spanning reads on RNAseq capture the fusion transcript, whereas junctional reads end at breakpoints and cannot be definitely attributed to the fusion. Expression analyses were therefore performed in the three primary cell lines derived from patients 1, 2, and 3 (sample details are listed in Supplementary Table S1). *BRAF* expression was significantly increased in fusion patient cell lines compared with that in a control melanocyte cell line (Hermes-1) (Figure 4a) but to a degree similar to that in cell lines derived from patients harboring the *NRAS* p.(Q61K) variant. In contrast, all three *BRAF*-fusion cell lines showed markedly increased levels of MAPK signaling activation compared with controls and the same *NRAS*-missense cell lines (Figure 4b).

BRAF-fusion cell lines are highly sensitive to trametinib treatment

Taking advantage of the three patient cell lines isolated in this study, we were able to assess their sensitivity to a MAPK/ extracellular signal–regulated kinase (ERK) kinase inhibitor (trametinib) treatment in vitro before translating its use to the clinic. Patient cell line proliferation was significantly sensitive to trametinib treatment, in a way similar to that of the control and the *NRAS* p.(Q61K) cell lines (Figure 5a and b). Most importantly, the decreased proliferation was accompanied by a significant reduction in MAPK signaling activation as measured by phosphorylation of ERK (Figure 5c).

Hyperproliferative phenotype of patients with CMN responds rapidly to oral MAPK/ERK kinase inhibitor treatment

On the basis of preliminary data, Great Ormond Street Hospital Drug and Therapeutics Committee approval was granted to trial trametinib in two patients with severe mosaic *BRAF*-fusion CMN. The first patient (who was not part of the original study), a boy aged 3 years, was referred to our department with a known *EVI5-BRAF* fusion. This patient exemplified the hyperproliferative and severely pruritic phenotype with a very bulky main CMN in a bathing trunk distribution, including affecting the genital area. The weight of the main CMN was considered to be impairing his gross motor development, including his ability to stand up from a sitting position. Sleep was being impaired by severe pruritus. Recurrent cutaneous infections within the main CMN were arising owing to the chronic inflammatory and hairless desmoplastic appearance of the surface of the lesion coupled with excoriations. Neurodevelopment was otherwise normal. The patient was started on 0.025 mg/kg/day trametinib given as 0.5 mg every other day. Within 4 weeks, there had been a visible reduction in CMN bulk, a reduction in erythema, and a reduction in pruritus. Within 12 weeks, there had been further visible and continued symptomatic improvement (Figure 5d), a reduction in overall body weight of 1 kg (equivalent to 6.6%) (Supplementary Figure S4), and clear improvement in gross motor ability. The only adverse effect
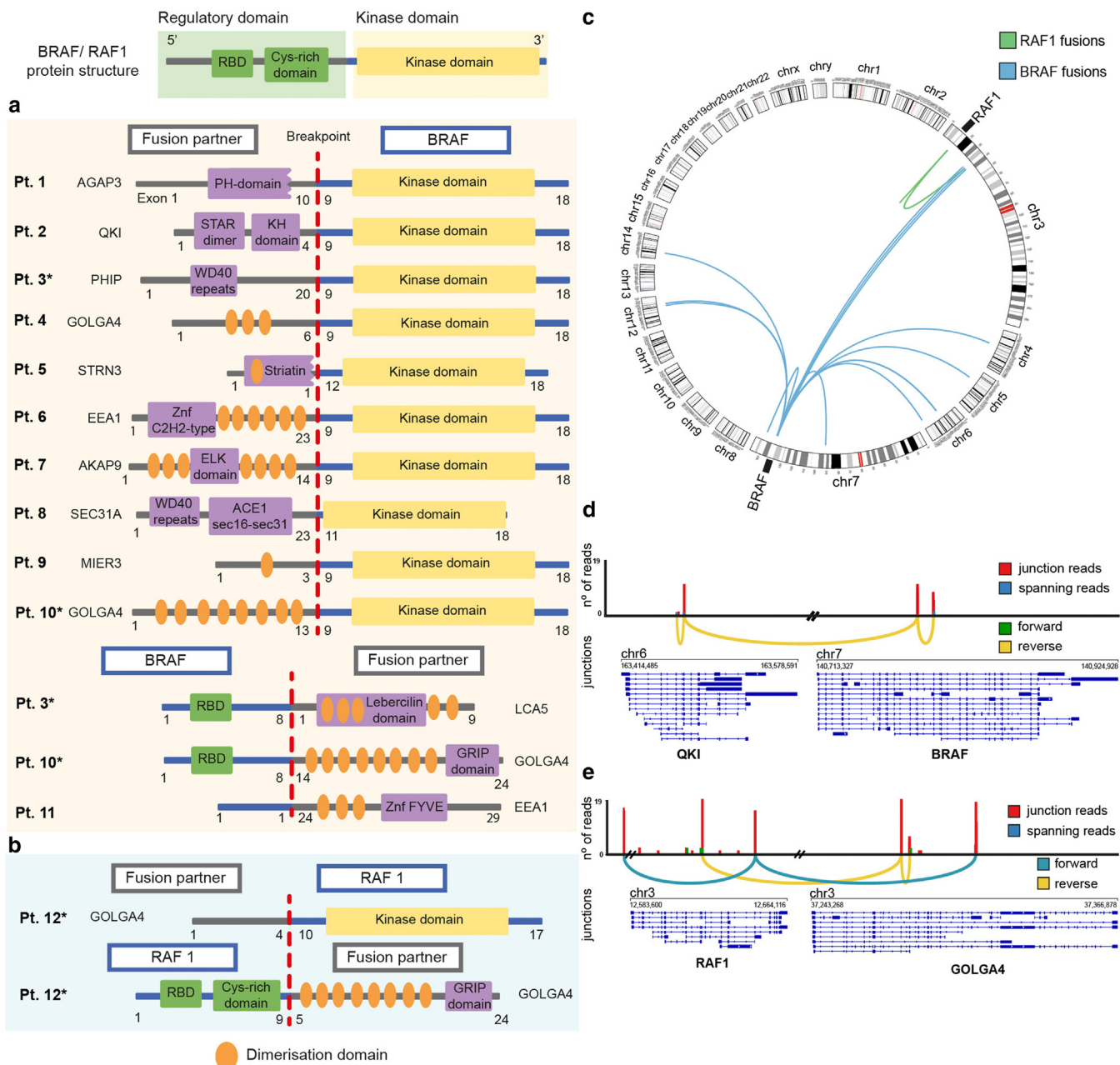
Figure 2. BRAF/RAF1 fusions identified in patients with CMN. Schematic illustration of the identified **(a)** *BRAF* and **(b)** *RAF1* fusions showing the wide range of fusion partners detected. Most fusions consist of the loss of the regulatory domain but retention of the *BRAF/RAF1* kinase domain. Recurrent *BRAF* breakpoints were identified in exon 9 (dotted red line), and relevant protein domains were identified using InterProScan. Asterisks highlight patients with more than one fusion. **(c)** Circos plot representation of *BRAF* and *RAF1* fusions identified by RNAseq. Sashimi plots showing **(d)** the single interchromosomal rearrangement of *BRAF* with the partner gene *QKI* found in patient 2 and **(e)** the complex complementary intrachromosomal rearrangement of *RAF1* with *GOLGA4* found in patient 12. Pt denotes patient. CMN, congenital melanocytic nevi; RNAseq, RNA sequencing.

seen during this time was a rise in creatine kinase, higher than baseline but only just outside the normal range and stable between weeks 4 and 8 and resolving by week 12. This rise in creatine kinase is recognized as a side effect of trametinib, and we have previously reported similar findings in the context of this drug in CMN syndrome where melanoma has arisen (Kinsler et al., 2017a). Patient 2, a girl aged 5 years with *QKI−BRAF* fusion, had a bulky, nodular CMN in the bathing trunk area with severe pruritis refractory to treatment with antihistamines and topical corticosteroids but no

obvious effects on motor development. She was commenced on trametinib at a dose of 0.025 mg/kg/day, equating to 0.5 mg on alternate days. Within 1 week, her pruritis was reported to have completely resolved, and within 4 weeks, she had a visible reduction in tissue CMN bulk and underlying erythema (Figure 5d). Again, there was a reduction in body weight noted at 1 month of treatment, with a 2.5 cm increase in height over the same period (Supplementary Figure S4). The only adverse effect was a slight increase in liver transaminases at 4 weeks, which is under review.
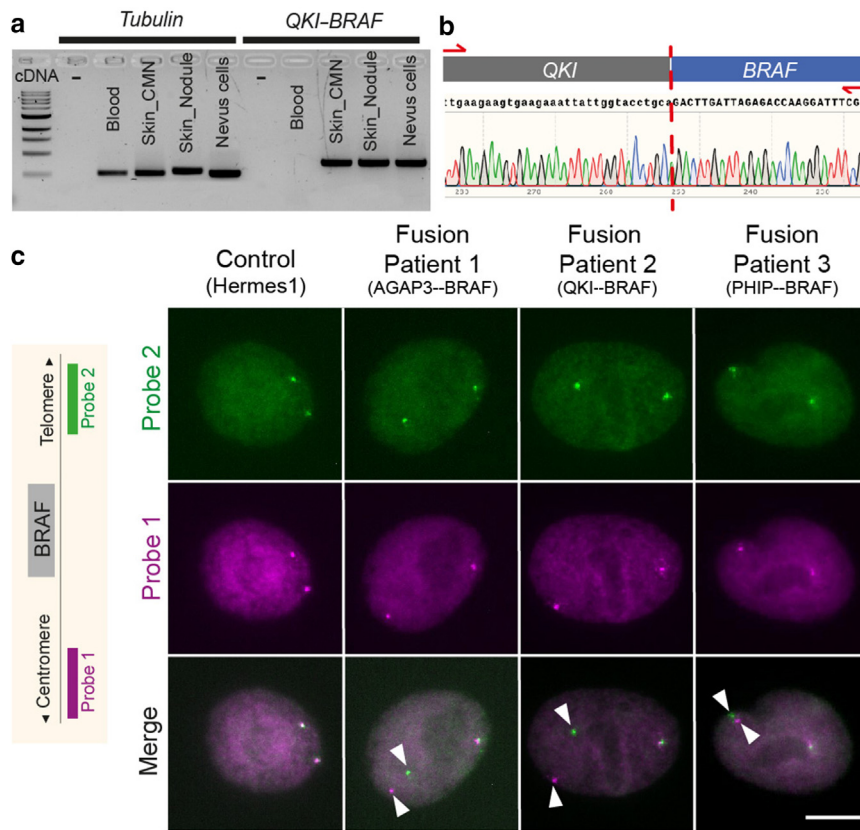
Figure 3. All *BRAF/RAF1* fusions were validated by additional methods. (a) Image of an agarose gel showing the PCR amplification of *QKI−BRAF* fusion transcript and the control tubulin in cDNA from the blood of patient 2, two different CMN lesions (main CMN and nodular area), and primary nevus cells. The fusion transcript was detected in the two lesions plus nevus cells but was absent in blood. **(b)** Sanger sequencing showing the breakpoint junction between *QKI* and *BRAF* (lowercase and uppercase nucleotides distinguish between *QKI* and *BRAF* fragments, respectively). **(c)** FISH using a *BRAF* breakapart probe demonstrating the presence of the *BRAF* rearrangement in three fusion patient cell lines (arrowheads) compared with that in the control cell line. Bar = 10 µm. CMN, congenital melanocytic nevi.

DISCUSSION

The finding of mosaic gene fusion events as a recurrent cause of the CMN phenotype described in this study may suggest that mosaic gene fusions could be considered a mechanism of disease in other congenital mosaic disorders, which are yet unexplained. We have provided a genotype to a further 7% (12 of 169) of patients with CMN in our cohort, and the functional exploration of the ensuing pathobiology has offered the rationale for targeted therapeutic intervention. Therefore, gene discovery in the field of mosaics continues to break ground in disease biology and to drive treatment for these severe conditions.

Detection using whole-genome RNAseq was relatively challenging at the bioinformatics level owing to the mosaic nature of the disease, together with a poor concordance between callers, a situation we are familiar with from detection of mosaic missense variants by DNA next-generation sequencing. Where nevus cell culture is possible, we would recommend the use of diagnostic breakapart probes as a relatively rapid method for detection, although this method is agnostic for the partner gene and does not give detailed information on breakpoints.

BRAF fusions are a well-described although relatively rare driver in different solid tumors, most commonly melanoma at approximately 3% (Botton et al., 2013; Forbes et al., 2015; Hutchinson et al., 2013; Ross et al., 2016). The fusions found in this study follow the same pattern as previously described, particularly with regard to the multiplicity of partner genes, and the presence of dimerization domains within those partner genes (Botton et al., 2013). *BRAF* fusions in melanoma are seen twice as commonly in females as in males, and this too has been mirrored in this small cohort of 11 patients (eight females). Given the parallel in a congenital disease, this sex difference is likely to reflect something
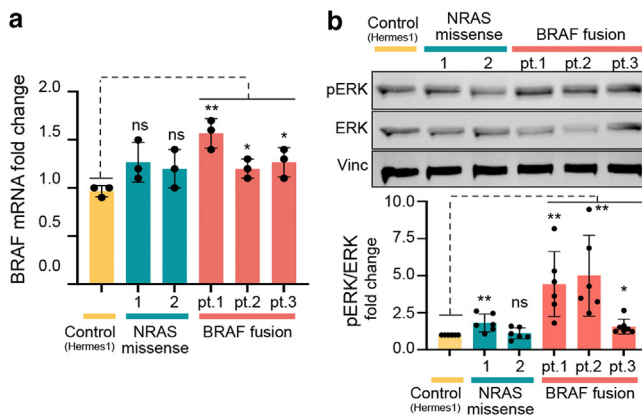

Figure 4. Increased *BRAF* expression and MAPK pathway activation in cell lines derived from patients with *BRAF* fusions. (a) Graph representing the significant increase in *BRAF* expression detected in fusion patient cell lines compared with that in control cell lines. **(b)** A significantly higher basal activation of the MAPK pathway was observed in fusion cell lines, detected by western blot, than in control cell lines. Only a representative blot, of the six independent ones performed to assess statistical differences, is shown. All statistical comparisons were performed by two-tailed unpaired *t*-test; *$P <$ 0.05, **$P <$ 0.01, ***$P <$ 0.001. pt. denotes patient. ERK, extracellular signal−regulated kinase; ns, not significant; pERK, phosphorylated ERK, extracellular signal−regulated kinase.
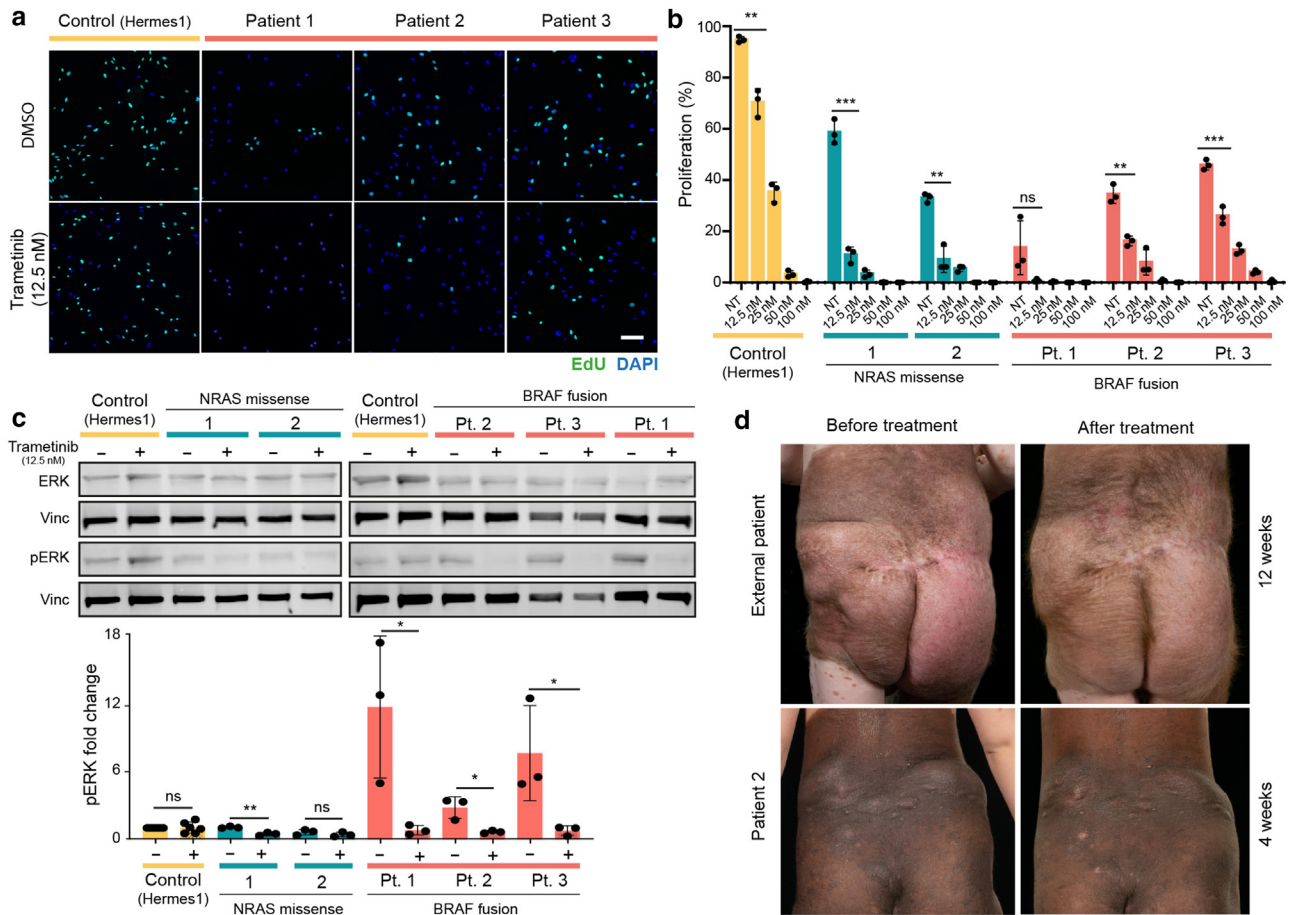
Figure 5. In vitro and in vivo response to trametinib (MEK inhibitor). (**a**) Control, *NRAS* variant, and *BRAF* fusion cell lines were treated with increasing concentrations of trametinib (12.5, 25, 50, 100 nM), and proliferation rates were assessed by EdU staining. (**b**) A significant decrease in proliferation was observed in all cell lines starting with the lowest trametinib concentration (12.5 nM) onward. (**c**) Significant reduction in MAPK activation levels after trametinib treatment (12.5 nM) in the three *BRAF*-fusion cell lines. (**d**) Clinical images of two patients before and after treatment with trametinib (0.025 mg/kg/day given as 0.5 mg every other day) reveal an improvement with a visible reduction in CMN bulk, a reduction in erythema, and a reduction in pruritus. All graphs represent an average of three independent experiments, and statistical comparisons were performed by two-tailed unpaired *t*-test; *$P < 0.05$, **$P < 0.01$, and ***$P < 0.001$. Bar = 100 μm. Pt denotes patient. CMN, congenital melanocytic nevi; EdU, 5-ethynyl-2′-deoxyuridine; MEK, MAPK/extracellular signal−regulated kinase kinase; NT, no treatment.

fundamental about the mechanisms underlying fusion generation rather than an environmental influence.

One patient had the same *RAF1* fusions in two CMN samples, demonstrating clonality, with two other cases previously described in the literature: one clonal (Martins da Silva et al., 2019) and one from more than one area of the same CMN, which had developed a rhabdomyosarcoma (Baltres et al., 2019). Taken together, these data likely support *RAF1* fusions as a recurrent cause of CMN. The patient with the *RAF1* fusion in this study does not have a hyperproliferative phenotype.

Given the recurrence of *BRAF* and *RAF1* in the gene fusions, these kinases are clearly key to the development of the nevus phenotype in these cases. However, a role or roles for the partner genes are also at least potentially contributory, particularly perhaps for the postnatal behavior where a few remain stable, but most become highly proliferative and pruritic. Expression levels of *BRAF* in *BRAF*-fusion nevus cells in culture were not substantially higher than in those with *NRAS* variants. Simply increased levels of expression driven by a more highly expressed partner gene is therefore not the whole story. Other than dimerization driving kinase activation, there could be other mechanisms through which the partner genes are involved in pathology, such as the spatiotemporal expression of the fusion proteins.

We have shown a statistically significant association between patients with *BRAF* fusion and a hyperproliferative phenotype; however, it is important to note the small total number in the cohort, so this remains to be confirmed in larger cohorts.

The pruritus in these cases is unresponsive to all nontargeted topical and oral medications we have tried so far. Alternative treatment for those patients is therefore highly desirable. Previous in vitro data from six melanoma cell lines harboring *BRAF* fusions demonstrated responsiveness to MAPK/ERK kinase inhibition (Botton et al., 2019), and two cases of *BRAF* fusion in single samples of CMN treated with oral trametinib demonstrated a reduction in the bulk and pruritus of the main lesion (Mir et al., 2019; Molho-Pessach et al., 2022). Our findings in vitro demonstrate high sensitivity of nevus cells in patients with *BRAF* fusion to trametinib, over and above that of *NRAS*-missense cells, and that

this sensitivity is due to quenching of MAPK hyperactivation. Our subsequent clinical data from the two patients described in this study demonstrates substantial and rapid clinical benefit from the first 4–12 weeks of oral trametinib, without clinically relevant side effects. However, importantly, this only treats the postnatal hyperproliferation and not the underlying congenital nevus, a similar situation to the tumor-specific effects of MAPK/ERK kinase inhibition seen in the treatment of melanoma in patients with CMN.

In conclusion, mosaic gene fusions are an important disease mechanism, and mosaic *BRAF* fusions and *RAF1* fusions are recurrent causes of CMN. Exploration of the biological effects of these fusions has demonstrated hyperactivation of the MAPK pathway over and above that of *NRAS*-missense CMN, by as yet unknown mechanisms, which could include dimerization of partner gene products. This translates clinically into a hyperproliferative and highly pruritic phenotype in most cases, which has been rapidly sensitive to oral trametinib administration in our trial patients. These studies have given a further 7% of patients a causative genotype and helped open the door to targeted therapies in this particularly severe phenotype.

MATERIALS AND METHODS

Patient recruitment and sample collection
All children with CMN seen in the pediatric dermatology department of a tertiary referral center between January 2015 and October 2020 were offered participation in a genotyping study, and written informed consent was obtained from their parents/guardians under the local National Health Service Research Ethics Committee (London Bloomsbury). No specific selection was done on the basis of the phenotypic characteristics (cohort details are provided in Supplementary Materials and Methods). CMN tissue was obtained either during routine surgery or by a single 4-mm punch skin biopsy for genotyping for *NRAS* and *BRAF* pathogenic variant hotspots and/or genotyping from archival formalin-fixed paraffin-embedded tissue as previously described (Polubothu et al., 2020). Parents/guardians consented to the publication of patient images.

RNAseq
Total RNA was extracted from CMN tissue of the 19 patients (sample details are listed in Supplementary Table S1) using the RNeasy Fibrous Tissue Mini Kit (74704, Qiagen, Hilden, Germany) according to the manufacturer's instructions. RNA integrity was assessed using a Bioanalyser (Agilent Technology, Santa Clara, CA). Library preparation using KAPA mRNA HyperPrep Kit with RiboErase (Roche, Basel, Switzerland) using 80 ng of total RNA and sequenced using a HiSeq (Illumina, San Diego, CA), with a 150-bp paired-end run at ∼40 million reads per lane, giving a total of ∼120 million (pairs of) reads per sample. Details of the alignment and bioinformatic analysis are available in Supplementary Materials and Methods.

Histology
H&E-stained formalin-fixed paraffin-embedded tissue sections from all available samples from each patient with *BRAF* fusion were reviewed by an independent expert histopathologist. Findings were reviewed in the context of recently published features of *BRAF*-fusion–acquired melanocytic nevi and in the context of the well-known histological features of *NRAS*-mosaic CMN (Yeh, 2023).

Nevus cell isolation and culture
Skin biopsies were collected from patients, as described in the sample collection section (sample details are listed in Supplementary Table S1), and transported fresh in a saline-soaked gauze to the laboratory within 2 hours. Detailed culturing and media preparation protocol is provided in Supplementary Materials and Methods.

Breakapart probe staining
BRAF breakapart probe was purchased from Empire Genomics (BRAFBA-20-ORGR). Patient cell lines (from patients 1, 2, and 3) were seeded, as detailed in Supplementary Materials and Methods, and staining was performed following the probe manufacturer's instructions. Representative images from n = 30 cells were taken with Zeiss Axio Imager M1.

Gene expression and western analyses
Patient-derived nevus cells (from patients 1, 2, and 3) were seeded in six-well plates at 0.5×10^6. Twenty-four hours later, RNA and protein were extracted from cell lysates to perform gene expression and pathway activation (western) analyses, respectively. A full detailed protocol is available in Supplementary Materials and Methods.

In vitro drug treatment
For proliferation studies, patient-derived nevus cells (from patients 1, 2, and 3) were seeded and treated 24 hours later with increasing concentrations of trametinib (12.5, 25, 50, and 100 nM), whereas only one concentration (12.5 nM) was used for pathway activation analyses (western). A full detailed protocol is available in Supplementary Materials and Methods.

Patient treatment
Two patients with *BRAF*-fusion CMN were recruited for treatment with trametinib after approval from the Great Ormond Street Hospital Drugs and Therapeutics Committee. Treatment dosing and monitoring schedule were as previously described (Kinsler et al., 2017b).

DATA AVAILABILITY STATEMENT
Raw RNA-sequencing data supporting the findings presented in this manuscript are available in ArrayExpress (https://www.ebi.ac.uk/biostudies/arrayexpress) under the accession number E-MTAB-13182

ORCIDs
Veronica A. Kinsler: http://orcid.org/0000-0001-6256-327X
Sara Barberan Martin: http://orcid.org/0000-0003-0142-4078
Satyamaanasa Polubothu: http://orcid.org/0000-0001-7195-5670
Alicia L. Bruzos: http://orcid.org/0000-0003-4362-545X
Alan Pittman: http://orcid.org/0000-0002-8112-2987
Gavin Kelly: http://orcid.org/0000-0001-7219-560X
Iwei Yeh: http://orcid.org/0000-0002-3941-3561
Neil Bulstrode: http://orcid.org/0000-0003-2617-7560
Pablo Lopez-Balboa: http://orcid.org/0000-0002-9944-719X
Aimie Sauvadet: http://orcid.org/0000-0002-8980-1239
Dale Bryant: http://orcid.org/0000-0002-4783-4796
Stuart Horswell: http://orcid.org/0000-0003-2787-1933
Davide Zecchin: http://orcid.org/0000-0002-4784-0336
Melissa Riachi: http://orcid.org/0000-0001-7278-1780
Fanis Michailidis: http://orcid.org/0000-0002-0408-3603
Amir Sadri: http://orcid.org/0000-0002-6084-2950
Noreen Muwanga-Nanyonjo: http://orcid.org/0009-0005-4772-4748
Nicole Knöpfel: http://orcid.org/0000-0002-6438-6550

CONFLICT OF INTEREST
The authors state no conflict of interest.

SUPPLEMENTARY MATERIAL

Supplementary material is linked to the online version of the paper at www.jidonline.org, and at https://doi.org/10.1016/j.jid.2023.06.213.

REFERENCES

Baltres A, Salhi A, Houlier A, Pissaloux D, Tirode F, Haddad V, et al. Malignant melanoma with areas of rhabdomyosarcomatous differentiation arising in a giant congenital nevus with RAF1 gene fusion. Pigment Cell Melanoma Res 2019;32:708−13.

Botton T, Talevich E, Mishra VK, Zhang T, Shain AH, Berquet C, et al. Genetic heterogeneity of BRAF fusion kinases in melanoma affects drug responses. Cell Rep 2019;29:573−88.e7.

Botton T, Yeh I, Nelson T, Vemula SS, Sparatta A, Garrido MC, et al. Recurrent BRAF kinase fusions in melanocytic tumors offer an opportunity for targeted therapy. Pigment Cell Melanoma Res 2013;26:845−51.

Dessars B, De Raeve LE, El Housni H, Debouck CJ, Sidon PJ, Morandini R, et al. Chromosomal translocations as a mechanism of BRAF activation in two cases of large congenital melanocytic nevi. J Invest Dermatol 2007;127:1468−70.

Etchevers HC, Rose C, Kahle B, Vorbringer H, Fina F, Heux P, et al. Giant congenital melanocytic nevus with vascular malformation and epidermal cysts associated with a somatic activating mutation in BRAF. Pigment Cell Melanoma Res 2018;31:437−41.

Forbes SA, Beare D, Gunasekaran P, Leung K, Bindal N, Boutselakis H, et al. COSMIC: exploring the world's knowledge of somatic mutations in human cancer. Nucleic Acids Res 2015;43:D805−11.

Houlier A, Pissaloux D, Tirode F, Lopez Ramirez N, Plaschka M, Caramel J, et al. RASGRF2 gene fusions identified in a variety of melanocytic lesions with distinct morphological features. Pigment Cell Melanoma Res 2021;34:1074−83.

Hutchinson KE, Lipson D, Stephens PJ, Otto G, Lehmann BD, Lyle PL, et al. BRAF fusions define a distinct molecular subset of melanomas with potential sensitivity to MEK inhibition. Clin Cancer Res 2013;19:6696−702.

Kent WJ, Sugnet CW, Furey TS, Roskin KM, Pringle TH, Zahler AM, et al. The human genome browser at UCSC. Genome Res 2002;12:996−1006.

Kinsler VA, Boccara O, Fraitag S, Torrelo A, Vabres P, Diociauti A. Mosaic abnormalities of the skin: review and guidelines from the European Reference Network for rare skin diseases. Br J Dermatol 2020;182:552−63.

Kinsler VA, O'Hare P, Bulstrode N, Calonje JE, Chong WK, Hargrave D, et al. Melanoma in congenital melanocytic naevi. Br J Dermatol 2017a;176:1131−43.

Kinsler VA, O'Hare P, Jacques T, Hargrave D, Slater O. MEK inhibition appears to improve symptom control in primary NRAS-driven CNS melanoma in children. Br J Cancer 2017b;116:990−3.

Kinsler VA, Thomas AC, Ishida M, Bulstrode NW, Loughlin S, Hing S, et al. Multiple congenital melanocytic nevi and neurocutaneous melanosis are caused by postzygotic mutations in codon 61 of NRAS [published correction appears in J Invest Dermatol 2016;136:2326] J Invest Dermatol 2013;133:2229−36.

Martins da Silva V, Martinez-Barrios E, Tell-Martí G, Dabad M, Carrera C, Aguilera P, et al. Genetic Abnormalities in Large to Giant Congenital Nevi: beyond NRAS mutations. J Invest Dermatol 2019;139:900−8.

Mir A, Agim NG, Kane AA, Josephs SC, Park JY, Ludwig K. Giant congenital melanocytic nevus treated with trametinib. Pediatrics 2019;143:e20182469.

Molho-Pessach V, Hartshtark S, Merims S, Lotem M, Caplan N, Alfassi H, et al. Giant congenital melanocytic naevus with a novel CUX1-BRAF fusion mutation treated with trametinib. Br J Dermatol 2022;187:1052−4.

Perron E, Pissaloux D, Neub A, Hohl D, Tartar MD, Mortier L, et al. Unclassified sclerosing malignant melanomas with AKAP9-BRAF gene fusion: a report of two cases and review of BRAF fusions in melanocytic tumors. Virchows Arch 2018;472:469−76.

Polubothu S, McGuire N, Al-Olabi L, Baird W, Bulstrode N, Chalker J, et al. Does the gene matter? Genotype-phenotype and genotype-outcome associations in congenital melanocytic naevi. Br J Dermatol 2020;182:434−43.

Ross JS, Wang K, Chmielecki J, Gay L, Johnson A, Chudnovsky J, et al. The distribution of BRAF gene fusions in solid tumors and response to targeted therapy. Int J Cancer 2016;138:881−90.

Salgado CM, Basu D, Nikiforova M, Bauer BS, Johnson D, Rundell V, et al. BRAF mutations are also associated with neurocutaneous melanocytosis and large/giant congenital melanocytic nevi. Pediatr Dev Pathol 2015;18:1−9.

Wei B, Gu J, Gao B, Bao Y, Duan R, Li Q, et al. Deficient mismatch repair is detected in large-to-giant congenital melanocytic naevi: providing new insight into aetiology and diagnosis. Br J Dermatol 2023;188:64−74.

Yeh I. Melanocytic naevi, melanocytomas and emerging concepts. Pathology 2023;55:178−86.

SUPPLEMENTARY MATERIALS AND METHODS

Patient cohort

The initial cohort used in this study consisted of 169 patients with congenital melanocytic nevi (134 included in a previous publication [Polubothu et al., 2020] plus 35 newly recruited between that publication and the time of this study). Of those 169 patients, 124 were *NRAS* mutant (73.4%), 7 were *BRAF* mutant (4.1%) and 38 were double wild type for *NRAS* and *BRAF* (22.5%). Of the 38 double wild-type patients, 19 had sufficient tissue available for RNA extraction and therefore were included in this study (phenotypic description is detailed in Supplementary Table S1). Statistical significance of the association between the presence of *BRAF/RAF1* fusions and the hyperproliferative phenotype was determined by a Fisher's exact test in Statistical Package for the Social Sciences (version 29.0.0.0).

Blood sampling

Peripheral blood samples were available from 8 of 19 patients and were collected and stored in Tempus Blood RNA tubes (Applied Biosystems, Waltham, MA) prior to RNA extraction using Tempus Spin RNA Isolation Kit (Applied Biosystems).

RNA-sequencing alignment and bioinformatics analysis

Raw data sequences were obtained in different sequencing runs, and read files belonging to the same sample were merged using in-house scripting. Quality of reads was assessed using FastQC, version 0.11.8, with Java-1.8 (https://www.bioinformatics.babraham.ac.uk/projects/ fastqc/). STAR-Fusion, version 1.6.0 (Dobin et al., 2013; Haas et al., 2019) was used to map RNA reads onto the Homo sapiens UCSC hg38 reference (GRCh38) genome and identify candidate fusion transcripts. Candidate fusions were then scored using FusionInspect, version 2.3.0, using junctions with at least one supporting read, at least three supporting novel junctions, and at least five spanning fragments. Read coverage for every RNA-sequencing sample was calculated using the featureCount tool of the subread package (Liao et al., 2014), version 1.6.4-foss-2018b, to obtain the fragments per kilobase of transcript per million mapped reads values. Only recurrent fusions (either within the cohort or between the cohort and the published literature) were selected for further investigation within this study. All the validated fusions had more than one supporting read.

Domains of predicted proteins were identified using InterProScan (Jones et al., 2014). Data visualization was performed with Circos (Krzywinski et al., 2009) and the Integrative Genomics Viewer (Robinson et al., 2011). Segmental duplications or LINE (long interspersed nuclear elements) and SINE (short interspersed nuclear elements) in the surroundings of the breakpoints of the gene fusions identified were annotated using the UCSC Genome Browser (Kent et al., 2002).

Nevus cell isolation and culture

The hypodermis was removed before the dermis/epidermis was incubated in a solution of PluriSTEM Dispase II (SCM133, Sigma-Aldrich, St. Louis, MO) containing 2.5 mM calcium chloride dihydrate (C7902, Sigma-Aldrich) and 1.5 U/ml collagenase D (11088858001, Roche, Basel, Switzerland) at 37 °C. After partial digestion (approximately 1 hour), the epidermis was separated from the dermis with forceps to continue the digestion of both components in separate tubes. When the tissues were adequately digested, they were resuspended in 5 ml Ham F-10 nutrient mix (11550043, Thermo Fisher Scientific, Waltham, MA) before separation through a 40-μm cell strainer (431750, Corning, Corning, NY) to remove aggregate material. The cells were pelleted at 250*g* for 5 minutes and separately resuspended and seeded in melanocyte growth medium. All cultures were incubated in a typical humidified, 37 °C, 5% carbon dioxide incubator, and the media was changed every 3—4 days.

Melanocyte growth medium. This included basal medium of Ham F-10 nutrient mix (11550043, Thermo Fisher Scientific), 20 ng/ml Stem cell factor (300-07, Peprotech, Rocky Hills, NJ), 5 ng/ml fibroblasts GF basic (100-18B, PeproTech), 50 ng/ml endothelin-1 (H-6995, Bachem, Bubendorf, Switzerland), 31.5 μM 3-isobutyl-1-methylxanthine (I5879, Sigma-Aldrich), 0.33 nM Cholera Toxin (C8052, Sigma-Aldrich), 5 nM phorbol 12-myristate 13-acetate (P8139, Sigma-Aldrich), 10 mg/ml Ultroser G (15950-017, Pall Life Sciences, New York, NW), 1x L-glutamine (25030024, Thermo Fisher Scientific), 1x penicillin-streptomycin (15070063, Gibco, Billings, MT), 1x amphotericin B (A2942, Sigma-Aldrich), and 2.5% v/v fetal bovine serum (10270106, Gibco).

The human immortalized melanocyte cell line (Hermes-1) was gifted by Downward Laboratory (Francis Crick Institute, London, United Kingdom) and was used as a control for all the experiments.

Breakapart probe staining

Control (Hermes-1) and patient cell lines (from patients 1, 2, and 3) were seeded in 60 mm dishes. After 24 hours, Colcemid (KaryoMAX, Gibco) was added to the media at concentration (10 μl/ml) and incubated for 45 minutes at 37 °C to arrest cells at metaphase. Subsequently, cells were harvested, pelleted, resuspended in 10 ml of hypotonic solution (0.075 M potassium chloride in water), and incubated at 37 °C for 20 minutes. A total of 2 ml of fixative (3:1 methanol:acetic acid) was added to the mixture before cells were pelleted and resuspended in 10 ml of fixative. Two additional washes with 5 ml fixative were performed before the cells were either stored at 4 °C or used for slide preparation. Slide preparation and staining were performed following the probe manufacturer's instructions.

Protein extraction and western blotting

Cell lysates were prepared in RIPA buffer supplemented with protease inhibitor cocktail (cOmplete Mini, Roche) and phosphatase inhibitor cocktail (PhosSTOP, Roche). Equal amounts of protein, as measured by BCA protein assay, were resolved in 4—15% Mini-Protean TGX gels (Bio-Rad Laboratories, Hercules, CA) and transferred onto Immobilon-FL PVDF membrane (Roche). Membranes were blocked for 1 hour at room temperature in 5% fish serum (gelatin from cold water fish skin; Sigma-Aldrich) before being incubated overnight at 4 °C with the primary antibodies diluted in BSA (Capricorn Scientific, Ebsdorfergrund, Germany). Secondary antibodies were diluted in Tris-buffered saline-0.1%Tween and incubated for 1 hour at room temperature. Detection of the signal was achieved using the Odyssey Infrared Imaging System (Odyssey, LI-COR Biosciences, Lincoln, NE). Western blot quantification was done using ImageStudioLite software.

The following antibodies were used at the indicated dilution: antiphosphorylated extracellular signal−regulated kinase (9101S, 1:1,000; Cell Signaling Technology, Danvers, MA), anti−extracellular signal−regulated kinase (9107S, 1:1,000; Cell Signaling Technology), anti-vinculin (MA5.11690, 1:5,000; Invitrogen, Waltham, MA), and secondary IRDye 800CW Goat anti-Mouse IgG (H+L) and IRDye 680CW Goat anti-Rabbit IgG (H+L) from LI-COR Biosciences.

Gene expression

RNA from cell lysates was extracted using RNAeasy Mini-Kit (Qiagen, Hilden, Germany) and 1 μg of RNA was used for High Capacity cDNA Reverse Transcription (Thermo Fisher Scientific). *BRAF* expression was measured by qRT-PCR using TaqMan Gene assay probe, identification 01052468.

In vitro drug treatment and cell proliferation

For proliferation experiments, control (Hermes-1) and patient-derived nevus cells were seeded in 96-well plates at a density of 3,500 cells/well. Twenty-four hours later, trametinib was added at different concentrations (12.5, 25, 50, 100 nM). Forty-eight hours after treatment, the drug was renewed and 5-ethynyl-2′-deoxyuridine was added at 10 μM. Cells were fixed and stained on day 6 following the manufacturer's instructions (ab219801, Abcam, Cambridge, United Kingdom).

For western blot, patient-derived nevus cells were seeded in six-well plates at 0.1×10^6 cells/well. After 24 hours, trametinib (6292, Cayman Chemical, Ann Arbor, MI) was added at 12.5 nM. Protein lysates were collected 5 days after treatment, with trametinib renewal done 48 hours after the first treatment.

SUPPLEMENTARY REFERENCES

Dobin A, Davis CA, Schlesinger F, Drenkow J, Zaleski C, Jha S, et al. STAR: ultrafast universal RNA-seq aligner. Bioinformatics 2013;29:15−21.

Haas BJ, Dobin A, Li B, Stransky N, Pochet N, Regev A. Accuracy assessment of fusion transcript detection via read-mapping and de novo fusion transcript assembly-based methods. Genome Biol 2019;20:213.

Jones P, Binns D, Chang HY, Fraser M, Li W, McAnulla C, et al. InterProScan 5: Genome-scale protein function classification. Bioinformatics 2014;30: 1236−40.

Kent WJ, Sugnet CW, Furey TS, Roskin KM, Pringle TH, Zahler AM, et al. The human genome browser at UCSC. Genome Res 2002;12:996−1006.

Krzywinski M, Schein J, Birol I, Connors J, Gascoyne R, Horsman D, et al. Circos: an information aesthetic for comparative genomics. Genome Res 2009;19:1639−45.

Liao Y, Smyth GK, Shi W. featureCounts: an efficient general purpose program for assigning sequence reads to genomic features. Bioinformatics 2014;30: 923−30.

Polubothu S, McGuire N, Al-Olabi L, Baird W, Bulstrode N, Chalker J, et al. Does the gene matter? Genotype-phenotype and genotype-outcome associations in congenital melanocytic naevi. Br J Dermatol 2020;182:434−43.

Robinson JT, Thorvaldsdóttir H, Winckler W, Guttman M, Lander ES, Getz G, et al. Integrative genomics viewer. Nat Biotechnol 2011;29:24−6.
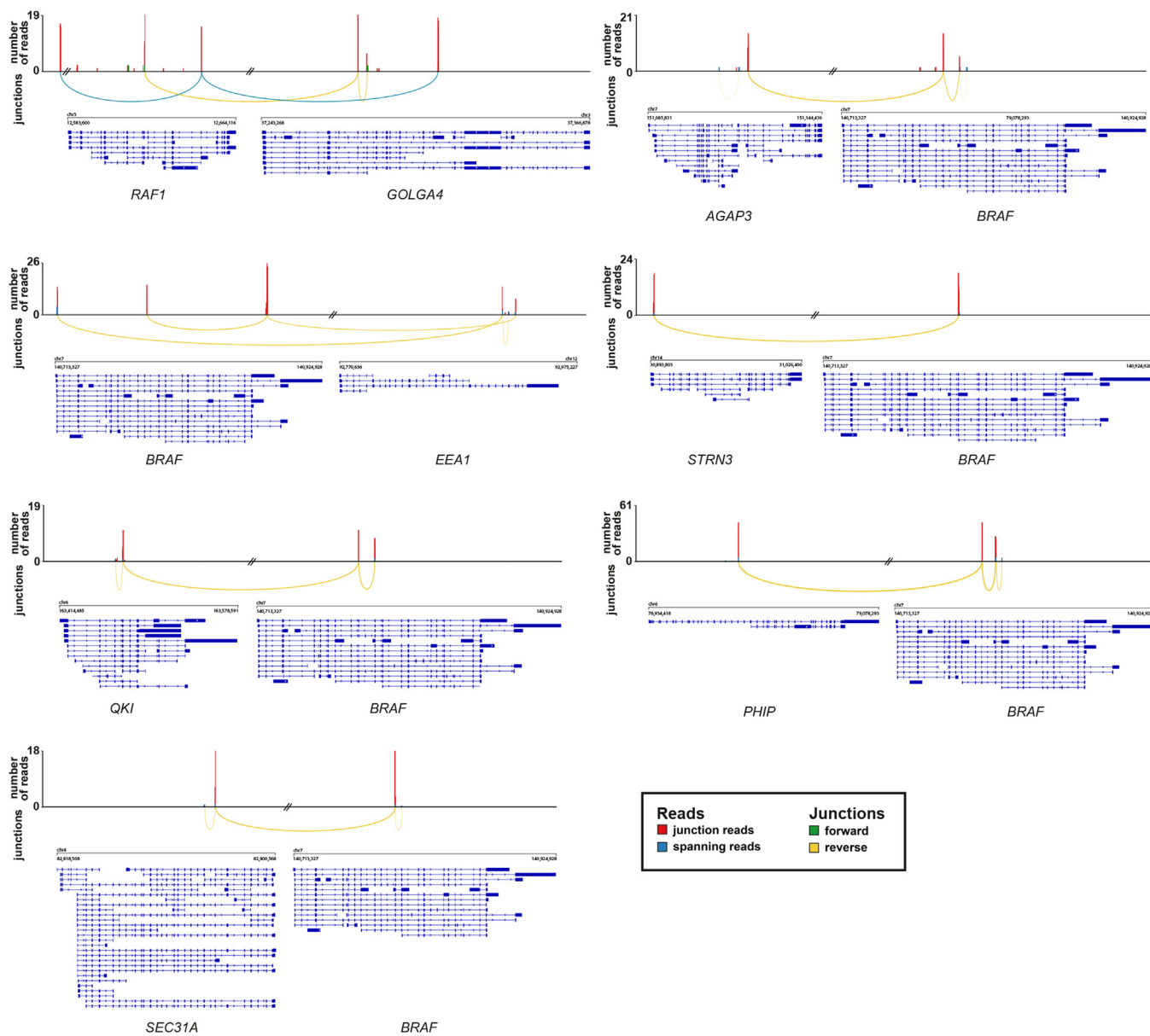
Supplementary Figure S1. Sashimi plots showing the junction and spanning reads supporting some of rearrangements. Sashimi plots could not be generated for 7 of 15 fusions owing to prediction problems. chr, chromosome.
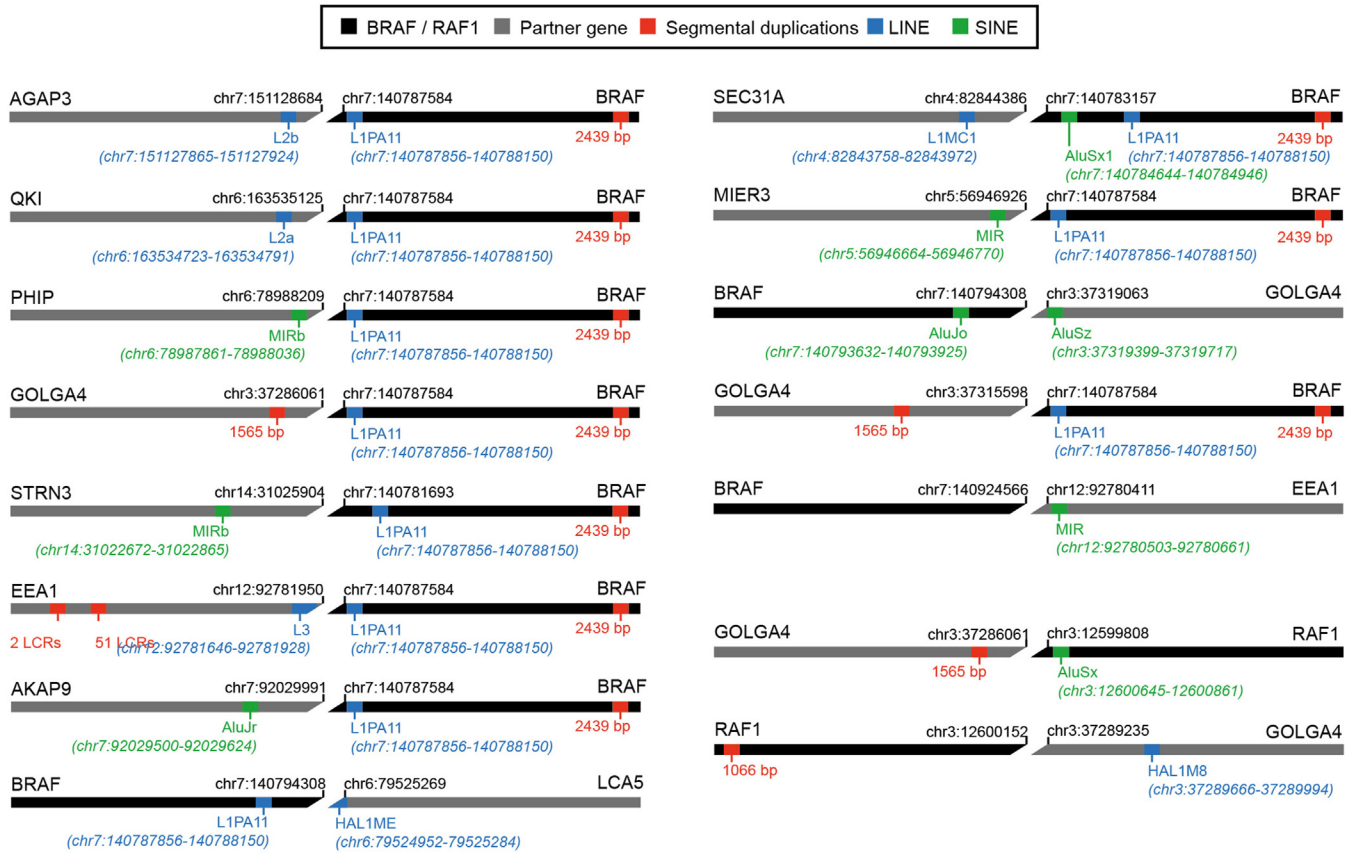
Supplementary Figure S2. Repeats annotation. Schematic representation of mosaic gene fusions identified in this study and the relevant repeats annotated in the surroundings of the breakpoints (not to scale) are shown. chr, chromosome; LINE, long interspersed nuclear element; SINE, short interspersed nuclear element.
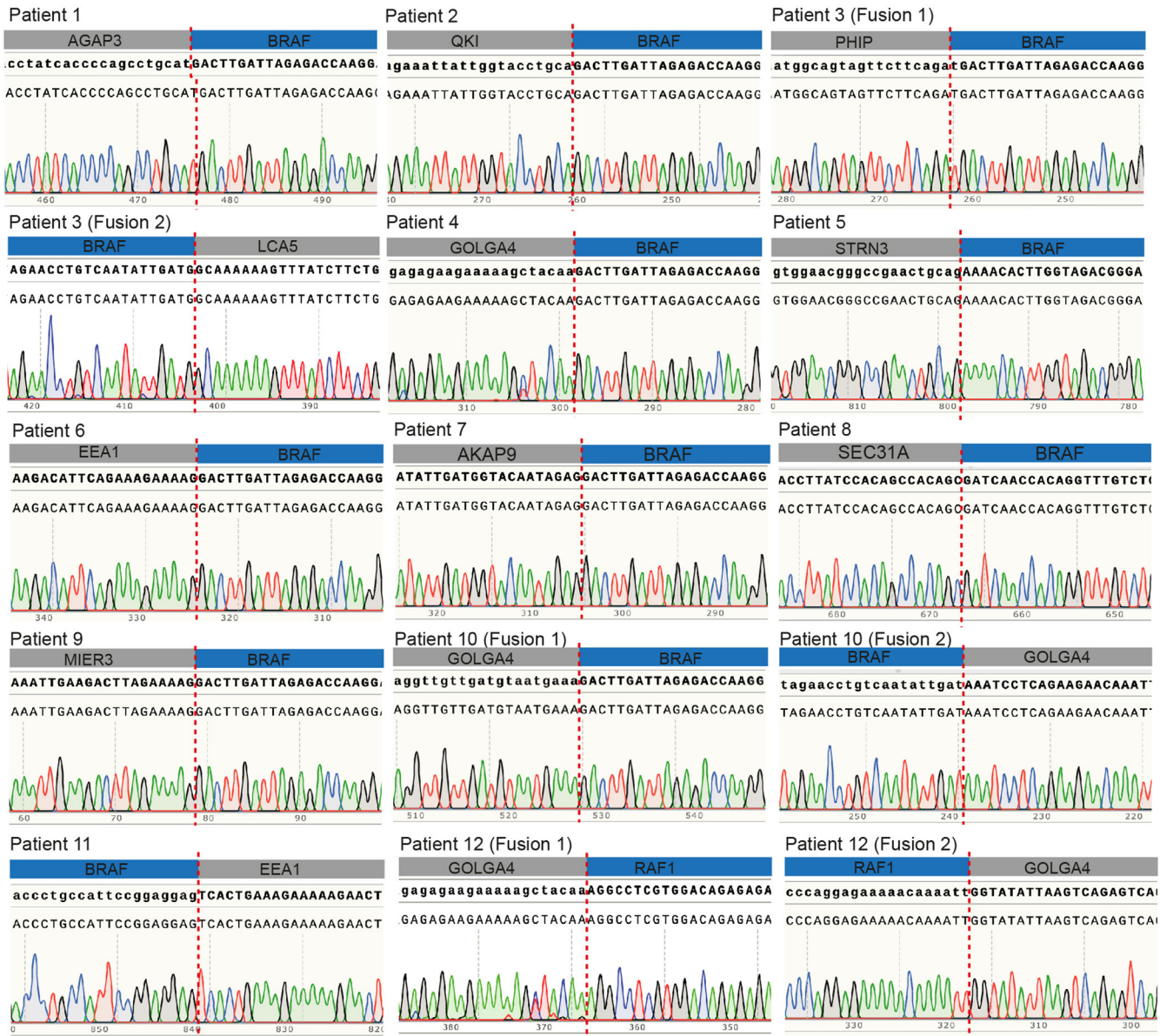
Supplementary Figure S3. Sequencing validation of all the fusions identified. Sanger sequencing traces demonstrating the presence of all the fusions identified by RNAseq are shown. The patient having each of the illustrated fusions is specified at the top of each panel. For patients having more than one fusion (patients 3, 10, and 12), this is indicated as fusion 1 or 2. *BRAF/RAF1* fragment is shown in blue, whereas the partner gene is shown in gray. The dotted line indicates the breakpoint. RNAseq, RNA sequencing.
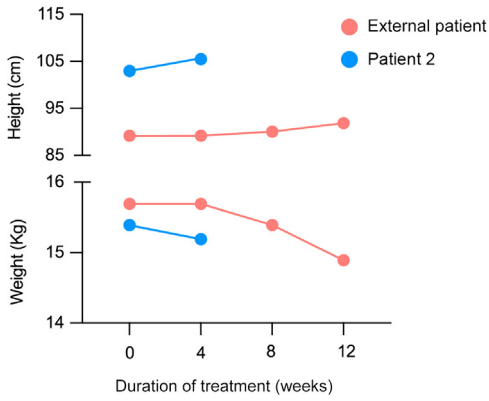
Supplementary Figure S4. Weight and height progression in the two patients treated with trametinib. Both patients show a reduction in overall body weight, despite an increase in height over the same period and without any other illnesses in the treatment period. The decrease in weight could therefore potentially be attributable to the visible decrease in CMN tissue bulk. CMN, congenital melanocytic nevi.

Supplementary Table S2. Detailed Histological Description of the Tissue Sections Reviewed

Patient Number	Number of Blocks Reviewed	Key Histopathologic Features
1	Six	1- epidermal acanthosis, pigmented melanocytes in papillary dermis. Interstitial pattern in reticular dermis with epithelioid melanocytes with expanded eosinophilic cytoplasm. 2- there is a cellular nodule of melanocytes within which the deep portion of the tumor is pigmented, and there are clusters of melanophages. 3- a nodular proliferation containing necrotized nests with pseudorosette-like structures. 4- cellular nodule of epithelioid melanocytes in the dermis 5- cellular nodule of epithelioid melanocytes in the dermis 6- histopathologic features similar to those of conventional congenital pattern nevus, with interstitial pattern in the reticular dermis. Areas of increased cellularity. Melanocytes extend into the septae of subcutis. Perivascular nests of melanocytes.
3	Two	1- exophytic configuration. Compound with nests of epithelioid melanocytes in the epidermis Cellular areas in the dermis and areas with pronounced neurotization, pseudo-Meissner corpuscles. 2- nevus and central proliferative nodule with slightly epithelioid melanocytes. Background nevus is not distinguishable from conventional *NRAS*-mutant congenital nevus. Image: proliferative nodule left, melanocytic nevus right.
4	Four	1- nodule of atypical epithelioid melanocytes within inflamed scar. One area has some features of BAP1 inactivation, with adjacent highly atypical nodules (melanoma vs. atypical proliferative nodule). Deep, there is an area of storiform fibrosis, perineurioma like. 2- scar 3- cyst 4- scar and small nevus
5	One	Cords within whorled fibrosis pattern. Junctional component. Some slightly spitzoid melanocytes in the papillary dermis. Delicate elongated rete ridges.
6	Nine (representative image shown in Figure 2f)	1-desmoplastic nevus with buckshot fibrosis 2- similar to 1 3- reactive lymph nodes 4- buckshot fibrosis pattern with low cellularity small clusters and single melanocytes with polygonal morphology and abundant cytoplasm 5-epithelioid melanocytes within dermal sclerosis 6- similar to 5 7- similar to 5 8- buckshot fibrosis pattern, with spitzoid epithelioid melanocytes and areas with cords in whorled fibrosis. 9- intermingled small and spitzoid melanocytes in one papillomatous lesion; the other shows buckshot fibrosis.
7	One (representative image shown in Figure 2e)	Cellular cords of melanocytes within whorled fibrosis. Superficial hyperpigmentation with junctional nests.
9	One	Whorled fibrosis, multinucleate melanocytes in the superficial portion. The melanocytes are slightly enlarged but not definitively spitzoid.
11	One (representative image shown in Figure 2d)	Domed exophytic skin segment shows cords in a whorled fibrosis pattern previously observed in acquired melanocytic tumors with *BRAF* fusion genes.

A total of 25 different blocks were reviewed from 8 of 12 patients with *BRAF* fusion.